Fusion barrier distribution derived from quasielastic excitation functions in ^{11}B, ^{12}C, ^{13}C+^{209}Bi reactions

P. K. Sahu, A. Saxena, B. K. Nayak, R. G. Thomas, B. V. John, and R. K. Choudhury
Nuclear Physics Division, Bhabha Atomic Research Centre, Mumbai 400085, India
(Received 17 February 2005; revised manuscript received 10 March 2006; published 21 June 2006)

The representations of fusion barrier distribution were derived from the quasielastic excitation function measured at the backward angle in ^{11}B, ^{12}C, ^{13}C+^{209}Bi reactions at energies around the Coulomb barrier. The experimental fusion barrier distributions were compared with the predictions of simplified coupled-channels fusion (CCDEF) calculations with inclusion of various channels coupling because of low-lying inelastic states of target and one and few nucleon transfers. The influence of neutron transfer coupling on fusion barrier distribution has been discussed.

DOI: 10.1103/PhysRevC.73.064604 PACS number(s): 25.70.Bc, 25.70.Hi, 25.70.Jj

I. INTRODUCTION

The heavy ion induced fusion reactions have been used frequently to understand the effect of projectile structure on the reaction dynamics [1,2]. The enhancement of subbarrier fusion cross section as compared to the one-dimensional barrier penetration model arises from coupling between the relative motion and intrinsic degree of freedom of the target and projectile. These degrees of freedom are nuclear deformation, inelastic excitation, particle transfers, projectile breakup, and many other multistep processes [3,4]. The coupled-channels models have been quite useful in explaining the enhancement of fusion cross section below the Coulomb barrier energies, as described in detail in Refs. [5,6] and references therein. The coupling can be described in terms of changes in the potential barrier between interacting bodies, leading to its splitting into several components around the one-dimensional barrier and thereby giving rise to a distribution of barriers. The lower ones being responsible for fusion at lower energies explain the enhancement at subbarrier energies. In other words, the shape of the barrier distribution can be directly linked to the coupling of channels that are important in governing the fusion process at energies around the barrier. In an earlier study, the enhancement of fusion cross section at subbarrier energies in ^{6}He+^{209}Bi, ^{238}U reactions as compared to that in ^{4}He+^{209}Bi, ^{238}U reactions were attributed because of breakup coupling of halo nuclei [7]. However, a systematic study on barrier distribution measured from fusion cross sections using ^{12}C, ^{16}O, ^{28}Si, and ^{35}Cl on ^{92}Zr [4] and comparison with the exact coupled-channels code CCFULL [8] without transfer channel coupling, suggested that the barrier distribution shape could have been reproduced better by including positive Q-value transfer channels present in the case of ^{28}Si- and ^{35}Cl-induced reactions. The enhancement in subbarrier fusion cross sections because of positive Q-value neutron transfer channels has been studied for ^{16,17}O+^{144}Sm [9], ^{32,36}S+^{110}Pd [10], ^{40}Ca+^{90,96}Zr [11], ^{40}Ca+^{46,48,50}Ti [12], and ^{16,18}O+^{120,124}Sn [13] systems. The fusion barrier distributions for ^{32,34}S+^{89}Y systems extracted from the measured fusion cross sections were explained by including the collectivity of the projectiles. Though the effect of proton transfer on the fusion process were found to be small in these reactions, the inclusion of coupling to positive Q-value proton stripping channels improved the fits to the low-energy cross sections [14]. The barrier distributions in ^{12}C+^{105,106}Pd and ^{13}C+^{105,106}Pd reactions have been studied using quasielastic excitation functions [15]. The low-Z projectiles and medium-Z targets were used in Ref. [15], where the coupling due to transfer channels could explain the barrier distributions much better as compared to the coupling due to the inelastic channels alone. This is possible because the effect of inelastic channels is hindered since the strength of the coupling to inelastic channels is proportional to the product of projectile and target atomic numbers. In the present work we have selected similar low-Z projectiles ^{11}B, ^{12}C, and ^{13}C but a high-Z target ^{209}Bi to see whether the transfer channels still play an important role in the barrier distribution inspite of large effect due to inelastic channels. The selected systems have diverse ground-state Q values and transfer strengths for transfer channels.

The fusion cross section ($\sigma_{\rm fus}$) for the heavy ion reaction under the adiabatic and isocentrifugal approximation can be written as a weighted sum of the fusion cross sections for a number of eigenchannels which depend on the direct reaction channel and couple strongly to the incident one [16,17]:

$$\sigma_{\rm fus}(E) = \sum_i W_i \sigma(E, B_i), \tag{1}$$

where W_i and B_i are the eigenchannel weights and barrier heights, with $\sum_i W_i = 1$. The multiple barriers present in the nuclear reactions as a result of coupling is directly extracted through a transformation of the experimental data. The distribution of potential barriers clearly showing the barrier structure can be obtained from the precise measurements of the experimental fusion cross section [15,18,19] as:

$$D_{\rm fus}(E) = \frac{1}{\pi r_b^2} \frac{d^2[E\sigma_{\rm fus}(E)]}{dE^2}. \tag{2}$$

This expression shows how a smooth fusion cross section can give rise to a distribution of barriers pertaining to various coupling involved in the collision of the two nuclei. This method is however not very sensitive at the high-energy part of the barrier distribution. Therefore, another widely used complementary approach to extract the representation

of barrier structure is by the measurement of quasielastic excitation function at the backward angles. This representation can be obtained from the first derivative of the ratio between quasielastic [$\sigma_{\rm qel}(E)$] and Rutherford [$\sigma_R(E)$] excitation function with respect to energy [11,20–23]:

$$D_{\rm qel}(E) = -\frac{d}{dE}\left[\frac{d\sigma_{\rm qel}(E)}{d\sigma_R(E)}\right], \quad (3)$$

where the quasielastic scattering cross section includes elastic, inelastic, and transfer channels. The measured fusion barrier distributions are sensitive to the target and projectile structure and the role of particle transfer leading to fusion which can be brought out by choosing different projectiles for the same target inelastic excitations [4]. The present selection of projectiles ^{11}B, ^{12}C, and ^{13}C on ^{209}Bi target will also help to bring out the relative importance of various transfer coupling in the representation of fusion-barrier distributions.

II. EXPERIMENT AND DATA ANALYSIS

The experiment was carried out using ^{11}B, ^{12}C, and ^{13}C beams from the 14 UD BARC-TIFR Pelletron accelerator facility in Mumbai. A ΔE (30 μm)-E (500 μm) silicon surface barrier detector telescope was mounted at an angle of 170° to the beam direction to detect the projectile-like fragments. Another silicon surface barrier detector telescope ΔE (35 μm)-E (1 mm) mounted at an angle of 40° with respect to the beam direction was used as the beam monitor for relative normalization of different runs. A self-supporting ^{209}Bi target of 500 μg/cm^2 thickness kept at normal angle with respect to the beam direction was used in the experiment. The measurements were carried out over the bombarding energy range of $E_{\rm lab}$ = 50–72 MeV and 40–62 MeV, respectively, for ^{12,13}C+^{209}Bi and ^{11}B+^{209}Bi systems in steps of 2-MeV intervals. The selected beam energy range were ±10 MeV around the Coulomb barrier. The bombarding energies have been corrected for the energy loss in half the target thickness, which are about 0.2 and 0.15 MeV, respectively, in ^{12,13}C+^{209}Bi and ^{11}B+^{209}Bi reactions. A typical two-dimensional ΔE-$E_{\rm Res}$ scatter plot from the detector telescope at back angle showing elastic and various transfer products (C, B, and Be) at $E_{\rm lab}$ = 64 MeV are shown in Fig. 1. The outgoing projectile-like fragments (PLF) of various charges are seen to be clearly separated. The quasielastic to Rutherford excitation functions were determined by using the expression:

$$\frac{d\sigma_{\rm qel}(E,\theta_{\rm tel})}{d\sigma_R} = \frac{N_{\rm tel}(E,\theta_{\rm tel})}{N_m(E,\theta_m)}\frac{[d\sigma_R/d\Omega](E,\theta_m)}{[d\sigma_R/d\Omega](E,\theta_{\rm tel})}\frac{\Delta\Omega_m}{\Delta\Omega_{\rm tel}},$$

where $\theta_{\rm tel}(\theta_m)$ is the fixed angle of the ΔE-E telescope (monitor) and $N_{\rm tel}$ (N_m) is the corresponding number of detected events of interest in the solid angle $\Delta\Omega_{\rm tel}$ ($\Delta\Omega_m$). The ratio $\Delta\Omega_m/\Delta\Omega_{\rm tel}$ was experimentally determined at low bombarding energies where the elastic scattering is expected to follow the Rutherford scattering. The number of events recorded in the area of ΔE-$E_{\rm Res}$ scatter plot associated with the quasielastic scattering channel, $N_{\rm tel}$, were taken by adding the number of events of PLF, having atomic number greater than 2. The quasielastic to Rutherford excitation functions so obtained for ^{12,13}C+^{209}Bi and ^{11}B+^{209}Bi systems are shown in Figs. 2(a) and (b) respectively.

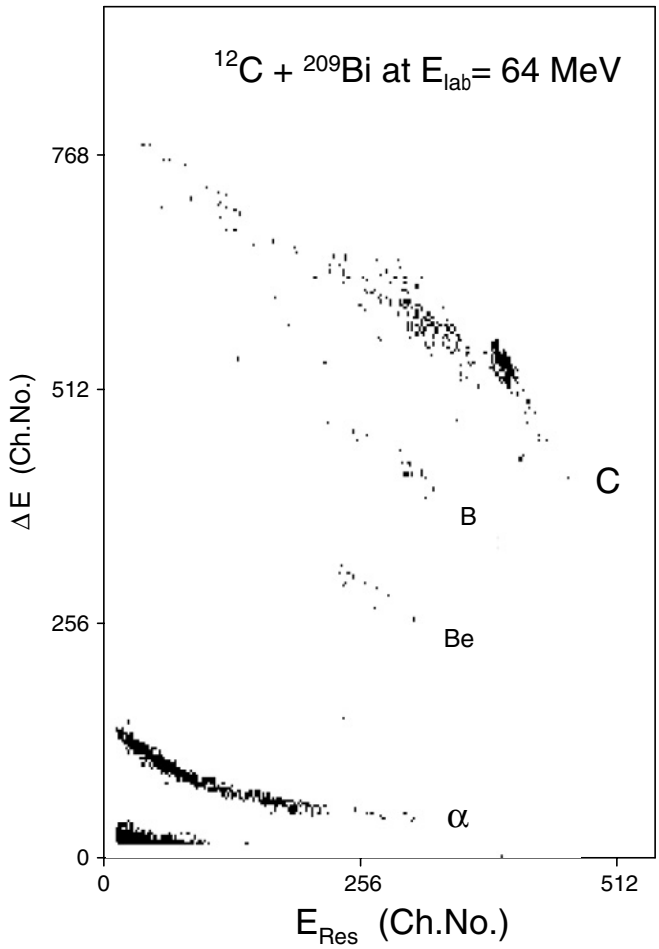

FIG. 1. A typical ΔE versus $E_{\rm Res}$ scatter plot for ^{12}C+^{209}Bi reactions at $E_{\rm lab}$ = 64 MeV. The outgoing projectile-like fragments (C, B, and Be) are identified.

III. DETERMINATION OF TRANSFER STRENGTH

In the present work we have reanalyzed our earlier data on transfer angular distributions [2] to determine the transfer strength, which goes as an input to the code CCDEF [24] for the inclusion of transfer coupling in the fusion cross-section calculation. The semiclassical method used in the present work have been described in Refs. [25–28]. In the present experiment the transfers to the individual states were not resolved, therefore the transfer probability after integration over Q from -∞ to the ground-state Q value (Q_{gg}) and assuming a Q-independent form factor can be written as a function of distance of closest approach (D) as

$$P(D) = \frac{\pi}{\sigma^2}|F(D)|^2\int_{-\infty}^{Q_{gg}} dQ\ \exp\left[-\frac{(Q-Q_{\rm opt})^2}{2\sigma^2}\right], \quad (4)$$

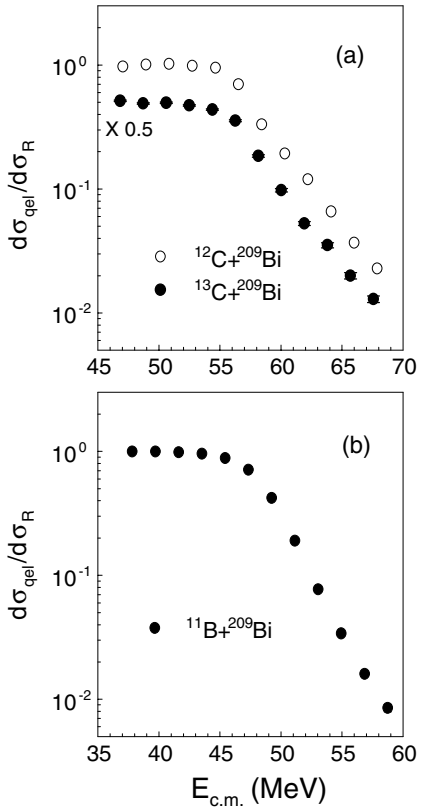

FIG. 2. The measured quasielastic excitation functions for ^{12,13}C+^{209}Bi and ^{11}B+^{209}Bi reactions at 170° laboratory angle.

where $\sigma = \sqrt{\hbar^2\alpha\ddot{r}_0/2}$, and $\ddot{r}_0$ [29] is the acceleration at D, given by

$$\ddot{r}_0 = \frac{Z_p Z_t e^2}{\mu D^2} \frac{1}{\sin(\theta_{c.m.}/2)}. \tag{5}$$

The binding-energy-derived decay constant α is given by a semiclassical relation $\alpha = \sqrt{2\mu E_B/\hbar^2}$, where E_B is the binding energy and μ is the reduced mass. The α was calculated as the average of the target and projectile after correcting for the binding energies [25] because of the Coulomb potential in the case of charged particle transfers. The optimum Q value, Q_{opt}, which is derived from the incoming and outgoing trajectory matching conditions [27], is given by

$$Q_{opt} = \left(\frac{Z_p^f Z_t^f}{Z_p^i Z_t^i} - 1\right) E_{c.m.}, \tag{6}$$

where i and f refer to the initial and final channels. The distance of closest approach, D in Eq. (4) is calculated by taking the average of incoming and outgoing elastic channels by assuming a Coulomb trajectory as given by

$$D = \frac{Z_p Z_t e^2}{2E_{c.m.}} \left[1 + \frac{1}{\sin(\theta_{c.m.}/2)}\right], \tag{7}$$

where Z_p and Z_t are the charges of projectile and target respectively and $E_{c.m.}$ is the center-of-mass energy. The experimental transfer probability $P_{expt}(D)$ is obtained by taking the ratio of the transfer cross section to the corresponding Rutherford cross section as

$$P_{expt}(D) = \frac{d\sigma_{tr}}{d\Omega} \Big/ \frac{d\sigma_R}{d\Omega}. \tag{8}$$

Here, $d\sigma_{tr}/d\Omega$ is the differential transfer cross section obtained from angular distribution data and $d\sigma_R/d\Omega$ is the calculated Rutherford cross section for the corresponding scattering angle θ. The $P_{expt}(D)$ as a function of distance of closest approach were obtained by converting the measured angular distribution for various transfer channels in ^{11}B, ^{12}C+^{209}Bi reactions at $E_{lab} = 69$ and 85 MeV, respectively; the experimental details of this experiment are reported in Ref. [2]. These data were fitted by the exponential function

$$P_{tr}(D) = P_{tr}(r_b)\exp[-2\alpha_t(D-r_b)], \tag{9}$$

with the free parameter α_t to obtain the transfer probabilities, $P_{tr}(r_b)$, at the Coulomb barrier radius r_b.

The $P_{expt}(D)$ for various transfer channels as a function of distance of closest approach along with the fits $P_{tr}(D)$ are shown in Fig. 3 for both the systems. The transfer form factor for various transfer channels at Coulomb barrier radius, $F(r_b)$, were calculated by using $P(D) = P_{tr}(r_b)$ in Eq. (4). The value of $F(r_b)$, Q_{gg}, α and the effective Q value (Q_{eff}) corrected for charged-particle transfers as $Q_{eff} = Q_{gg} - Q_{opt}$ are listed in Table I for ^{11}B+^{209}Bi and ^{12}C, ^{13}C+^{209}Bi systems at $E_{lab} = 69$ and 85 MeV, respectively. The transfer strengths for various transfer channels in ^{13}C+^{209}Bi reaction were assumed to be the same as that calculated for the corresponding number of particle transfers in ^{12}C+^{209}Bi reaction, because the experimental transfer probabilities were not measured in the former case; however, it was varied for the important positive Q-value transfer channels. The + and − signs indicate the particle pickup and stripping by projectile with respect to target.

TABLE I. Table containing Q_{gg}, Q_{eff}, α, and $F(r_b)$ for various transfer channels in ^{12}C, ^{13}C+^{209}Bi, and ^{11}B+^{209}Bi reactions at $E_{lab} = 85$ and 69 MeV, respectively.

Systems	Channel	Q_{gg} (MeV)	Q_{eff} (MeV)	α (fm^{-1})	$F(r_b)$ (MeV)
^{12}C+^{209}Bi	$+1n$	−2.51	−2.51	0.53	1.04
	$+2n$	−1.25	−1.25	1.10	0.19
	$-1p$	−10.97	1.63	0.82	0.48
	$-1p1n$	−17.87	−5.27	1.12	0.12
	$-2p$	−19.2	6.3	1.49	0.19
^{13}C+^{209}Bi	$+1n$	−0.74	−0.74	0.60	
	$+2n$	4.95	4.95	1.03	
	$-1p$	−12.60	−0.07	0.84	
	$-1p1n$	−11.38	1.15	1.24	
	$-2p1n$	−12.43	12.96	1.86	
^{11}B+^{209}Bi	$+1p$	12.16	0.00	0.79	0.20
	$-1n$	−6.85	−6.85	0.58	0.40
	$+1n$	−4.09	−4.09	0.49	0.59
	$-1p$	−6.24	6.23	1.70	0.35
	$-1p1n$	−8.50	3.97	1.18	0.12

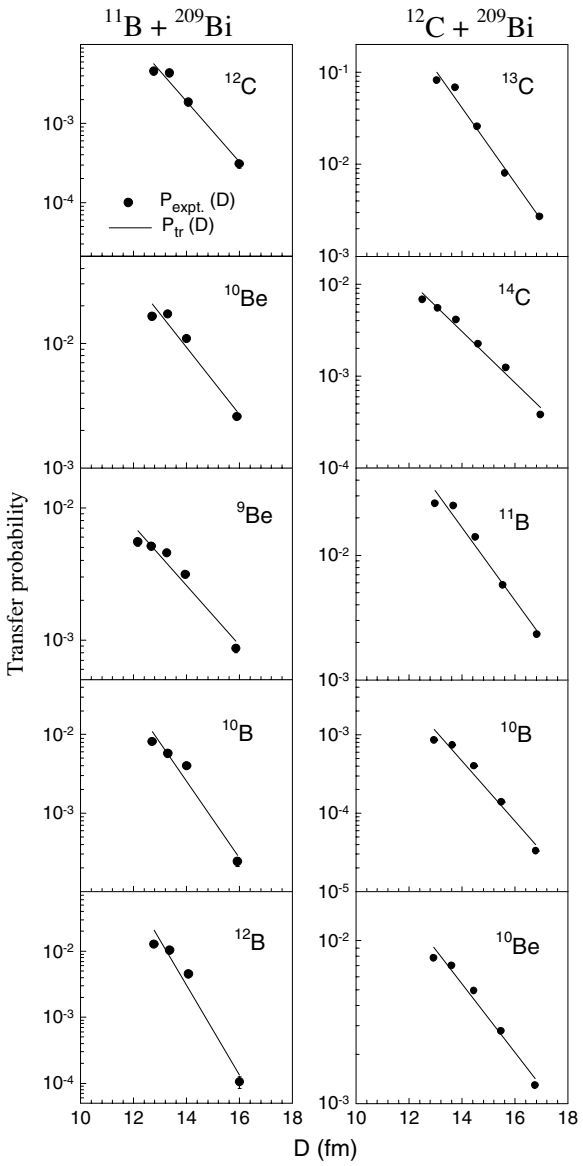

FIG. 3. Transfer probabilities as a function of distance of closest approach, along with the exponential fits, using Eq. (9) for various transfer channels in ^{11}B+^{209}Bi and ^{12}C+^{209}Bi reactions at $E_{\rm lab} = 69$ and 85 MeV, respectively.

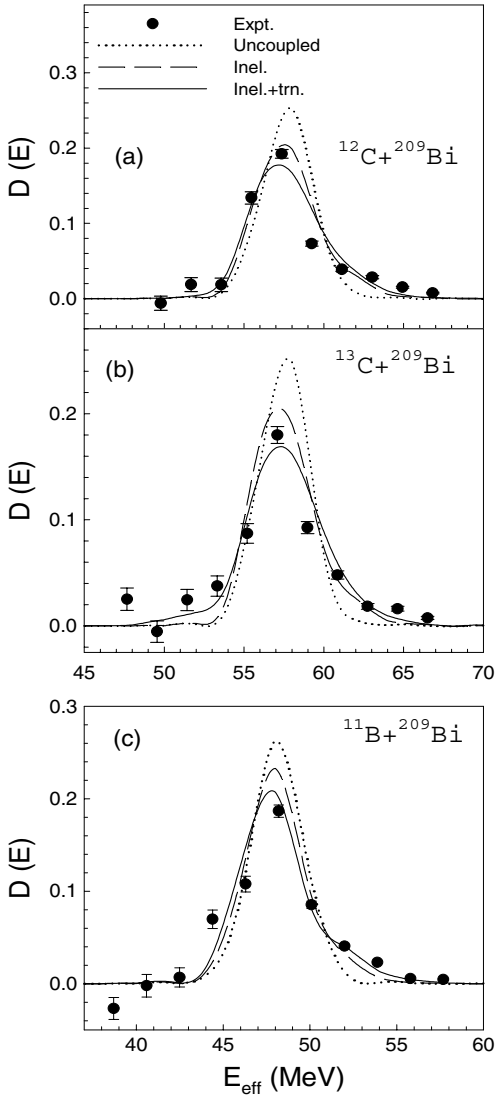

FIG. 4. Representation of fusion barrier distribution for ^{12}C, ^{13}C, ^{11}B+^{209}Bi systems along with the simplified coupled-channels calculations for various coupling conditions. The dotted lines represent the without coupling cases, the dashed lines show coupling of target inelastic excitations, and the solid lines show coupling of both inelastic and transfer channels as listed in Table I.

IV. RESULTS AND DISCUSSIONS

The experimental barrier distributions (BD) were obtained by taking first derivative of $d\sigma_{\rm qel}/d\sigma_R$ with respect to energy by using a point difference formula. In order to compare the shape of $D_{\rm qel}(E, \theta = 170^\circ)$ with that of $D_{\rm qel}(E, \theta = 180^\circ)$, the energy scale of the former was reduced by the centrifugal energy [11] $E_{\rm cent}$ given by

$$E_{\rm cent} = E_{\rm c.m.} \frac{{\rm cosec}(\theta_{\rm c.m.}/2) - 1}{{\rm cosec}(\theta_{\rm c.m.}/2) + 1}, \qquad (10)$$

the reduced energy $E_{\rm eff}$ is used as $E_{\rm c.m.} - E_{\rm cent}$. The experimental BD for ^{12}C, ^{13}C+^{209}Bi and ^{11}B+^{209}Bi systems are shown by solid dots in Figs. 4(a)–(c), respectively. The fusion cross sections were calculated with and without coupling of various inelastic and transfer channels by using the simplified coupled-channels code CCDEF. The fusion BD were obtained from the fusion excitation functions using Eq. (2). The calculated fusion barrier distribution was normalized by a factor $d(E\sigma_{\rm fus})/dE$ at higher energies where it reaches a saturation that corresponds to the πr_b^2 value of the corresponding system. The bare nuclear fusion potential parameters were obtained by varying the depth of the Woods-Saxon potential for uncoupled case to reproduce the average position of the experimental BD. The Coulumb barrier V_b, barrier position r_b, $\hbar\omega$ the s-wave curvature at r_b, mean and variance of the experimental barrier destributions are listed in Table II. The experimental values of mean and variance of the BD are also listed in Table II. It is observed that the variance of the BD increases as a function of charge and mass of the

TABLE II. The Coulomb barrier V_b, barrier position r_b, $\hbar\omega$ the s-wave curvature at r_b, mean and variance of the experimental barrier distributions.

Systems	V_b (MeV)	r_b (fm)	$\hbar\omega$ (MeV)	Mean (MeV)	Variance (MeV^2)
^{11}B+^{209}Bi	48.1	11.72	4.73	48.1	7.96
^{12}C+^{209}Bi	57.7	11.72	4.94	57.7	8.88
^{13}C+^{209}Bi	57.5	11.76	4.72	57.5	9.36

projectile. The dotted lines in Figs. 4(a)–(c) are the uncoupled or one-dimensional barrier-penetration-model calculations for ^{12}C+^{209}Bi, ^{13}C+^{209}Bi, and ^{11}B+^{209}Bi systems, respectively. For the uncoupled cases, the calculated BD peaks are narrow, high, symmetric, and structureless. To explain the shape of the tails of the experimental BD on the high-energy side of ^{12}C, ^{11}B+^{209}Bi systems and both low- and high-energy side of ^{13}C+^{209}Bi system seem to require the presence of some coupling to other channels such as inelastic and/or transfer in CCDEF calculations.

The inelastic excitation coupling strength included in the coupled-channels calculation is given by

$$F_{\rm inel}(r) = \frac{\beta_\lambda}{\sqrt{4\pi}}\left[-R\frac{dV_n(r)}{dr} + \frac{3Z_pZ_te^2}{2\lambda+1}\frac{R^\lambda}{r^{\lambda+1}}\right], \quad (11)$$

where R and β_λ are the radius and deformation parameter of the excited nucleus, λ the transition multipolarity, and V_n the nuclear potential [24]. The inelastic coupling included in the calculations are the lowest 3^- ($\beta_3 = 0.122$, $E_x = 2.62$ MeV), 2^+ ($\beta_2 = 0.05$, $E_x = 4.18$ MeV), and 5^- ($\beta_5 = 0.0802$, $E_x = 3.09$ MeV) states of ^{209}Bi that are treated in the vibrational model [30]. The deformation parameter used for the above inelastic states are that of the ^{208}Pb instead of ^{209}Bi, which is valid in the framework of weak coupling approximation. The predictions of CCDEF with the inclusion of coupling due to inelastic channels are shown by dashed lines for ^{12}C+^{209}Bi, ^{13}C+^{209}Bi, and ^{11}B+^{209}Bi systems in Figs. 4(a)–(c) respectively.

The coupled-channels calculations including only the target inelastic excitations are reasonably able to explain the barrier distribution in ^{12}C+^{209}Bi reaction; however, it is not able to completely reproduce the fusion BD structures in ^{13}C, ^{11}B+^{209}Bi reactions. It is also known that the high-lying states with excitation energies comparable to the curvature of the fusion barrier do not effect the structure of the barrier distribution but rather only give an overall shift to the barrier position [3]. Hence, we have not considered the coupling of projectile inelastic states in the present analysis. It is therefore necessary to introduce additional channels coupling in terms of one- and few-nucleon transfers in the fusion coupled-channels calculations for a better comparison with the experimental data.

The transfer channels couplings were included in the code CCDEF with α, $Q_{\rm eff}$, and $F(r_b)$ values as listed in Table I for the ^{12}C, ^{13}C+^{209}Bi, and ^{11}B+^{209}Bi reactions. In the case of ^{12}C+^{209}Bi reaction, inclusion of all the transfer channels ($+1n$, $+2n$, $-1p$, $-1p1n$, and $-2p$) couplings has a minor effect on the overall shape of the barrier distribution except for a small increase in the width of the barrier distribution, as shown in Fig. 4(a) by the solid line. In the case of ^{13}C+^{209}Bi reaction, inclusion of all the transfer channels ($+1n$, $+2n$, $-1p$, $-1p1n$, and $-2p1n$) coupling improves the comparison between the experimental and CCDEF prediction for high energy side of the barrier distribution. However, to reproduce the lower-energy side of the experimental barrier distribution, it was required to increase the strength of the positive Q-value ($+2n$) channel to 1.2, as shown in Fig. 4(b) by the solid line. It is observed that the main contributions are due to the ($+1n$) and ($+2n$) transfer channels at the higher- and lower-energy sides of the barrier distribution, respectively, whereas other transfer channels are found to have a negligible effect on the overall structure of the barrier distribution. In the case of ^{11}B+^{209}Bi reaction, the coupling of all the transfer channels listed in Table I were included in the coupled-channels calculation. The shape of the barrier distribution showed a very small improvement even after including all the transfer channels. Though the ($+1n$) and ($-1n$) transfer channels have similar Q values and strengths, increasing the strength of ($-1n$) channel does not explain the higher side of the barrier distribution. However, by increasing the transfer strength of the ($+1n$) channel to twice the value as listed in Table I, the peak and high-energy part of the barrier distribution is well explained, as shown in Fig. 4(c) by the solid line. The present work indicates the important role of transfer channels toward the overall structure of the barrier distribution despite a large contribution because of inelastic channels.

V. SUMMARY AND CONCLUSION

The quasielastic excitation functions were measured at the backward angle and the representation of fusion barrier distributions were obtained for ^{12}C, ^{13}C+^{209}Bi, and ^{11}B+^{209}Bi reactions around 10 MeV below and above the Coulomb barrier. The transfer strengths were extracted for ^{12}C, ^{11}B+^{209}Bi reactions from the transfer probability measurement using a semiclassical method. The experimental BD were compared with coupled channels predictions using both inelastic and transfer channels coupling. In the case of ^{12}C+^{209}Bi reaction the inelastic channels are good enough to explain the overall barrier distribution. In the case of ^{13}C+^{209}Bi reaction the coupling of ($+1n$) and ($+2n$) transfer channels are found to be important to explain the overall structure of barrier distribution, whereas the coupling of other charged-particle transfer channels have a negligible effect on the barrier distribution. In the case of ^{11}B+^{209}Bi reaction the shape of barrier distribution is better reproduced by increasing the coupling strength of ($+1n$) transfer channels.

ACKNOWLEDGMENTS

The authors thank Dr. P. Shukla, Mr. V. Jha, and Mr. Y. S. Sawant for their help during the experiment and for useful discussions. The authors also thank Mr. A. Inkar and Mr. R. V. Jangale for their help during the experiment. The assistance from the operation staff of the Pelletron accelerator is gratefully acknowledged.

[1] P. K. Sahu, R. K. Choudhury, D. C. Biswas, and B. K. Nayak, Phys. Rev. C **64**, 014609 (2001).
[2] P. K. Sahu, A. Saxena, R. K. Choudhury, B. K. Nayak, D. C. Biswas, L. M. Pant, R. G. Thomas, and Y. S. Sawant, Phys. Rev. C **68**, 054612 (2003).
[3] M. Dasgupta, D. J. Hinde, N. Rowley, and A. M. Stefanini, Annu. Rev. Nucl. Part. Sci. **48**, 401 (1998).
[4] J. O. Newton, C. R. Morton, M. Dasgupta, J. R. Leigh, J. C. Mein, D. J. Hinde, H. Timmers, and K. Hagino, Phys. Rev. C **64**, 064608 (2001).
[5] M. Beckerman, Rep. Prog. Phys. **51**, 1047 (1988).
[6] A. B. Balantekin and N. Takigawa, Rev. Mod. Phys. **70**, 77 (1998).
[7] N. Alamanos, A. Pakou, V. Lapoux, J. L. Sida, and M. Trotta, Phys. Rev. C **65**, 054606 (2002).
[8] K. Hagino, N. Rowley, and A. T. Kruppa, Comput. Phys. Commun. **123**, 143 (1999).
[9] C. R. Morton, M. Dasgupta, D. J. Hinde, J. R. Leigh, R. C. Lemmon, J. P. Lestone, J. C. Mein, J. O. Newton, H. Timmers, N. Rowley, and A. T. Kruppa, Phys. Rev. Lett. **72**, 4074 (1994).
[10] A. M. Stefanini, D. Ackermann, L. Corradi, J. H. He, G. Montagnoli, S. Beghini, F. Scarlassara, and G. F. Segato, Phys. Rev. C **52**, R1727 (1995).
[11] H. Timmers, D. Ackermann, S. Beghini, L. Corradi, J. H. He, G. Montagnoli, F. Scarlassara, A. M. Stefanini, and N. Rowley, Nucl. Phys. **A633**, 421 (1998).
[12] A. A. Sonzogni, J. D. Bierman, M. P. Kelly, J. P. Lestone, J. F. Liang, and R. Vandenbosch, Phys. Rev. C **57**, 722 (1998).
[13] S. Sinha, M. R. Pahlavani, and R. Varma, R. K. Choudhury, B. K. Nayak, and A. Saxena, Phys. Rev. C **64**, 024607 (2001).
[14] A. Mukherjee, M. Dasgupta, D. J. Hinde, K. Hagino, J. R. Leigh, J. C. Mein, C. R. Morton, J. O. Newton, and H. Timmers, Phys. Rev. C **66**, 034607 (2002).
[15] O. A. Capurro, J. E. Testoni, D. Abriola, D. E. DiGregorio, G. V. Marti, A. J. Pacheco, M. R. Spinella, and E. Achterberg, Phys. Rev. C **62**, 014613 (2000).
[16] K. Hagino, N. Takigawa, and A. B. Balantekin, Phys. Rev. C **56**, 2104 (1997).
[17] E. Piasecki *et al*., Phys. Rev. C **65**, 054611 (2002).
[18] N. Rowley, G. R. Satchler, and P. H. Stelson, Phys. Lett. **B254**, 25 (1991).
[19] J. R. Leigh, M. Dasgupta, D. J. Hinde, J. C. Mein, C. R. Morton, R. C. Lemmon, J. P. Lestone, J. O. Newton, H. Timmers, J. X. Wei, and N. Rowley, Phys. Rev. C **52**, 3151 (1995).
[20] K. Hagino and N. Rowley, Phys. Rev. C **69**, 054610 (2004).
[21] O. A. Capurro, J. E. Testoni, D. Abriola, D. E. DiGregorio, J. O. Fernandez Niello, G. V. Marti, A. J. Pacheco, M. R. Spinella, M. Ramirez, C. Balpardo, and M. Ortega, Phys. Rev. C **65**, 064617 (2002).
[22] R. Varma, S. Sinha, B. K. Nayak, R. G. Thomas, A. Saxena, D. C. Biswas, L. M. Pant, D. M. Nadkarni, R. K. Choudhury, and P. Bhattacharya, Phys. Rev. C **57**, 3462 (1998).
[23] H. Timmers, J. R. Leigh, M. Dasgupta, D. J. Hinde, R. C. Lemmon, J. C. Mein, C. R. Morton, J. O. Newton, and N. Rowley, Nucl. Phys. **A584**, 190 (1995).
[24] J. Fernandez-Niello, C. H. Dasso, and S. Landowne, Comput. Phys. Commun. **54**, 409 (1989).
[25] R. A. Broglia and A. Winther, *Heavy Ion Reactions* (Addison-Wesley, Reading, MA, 1991), Vol. I.
[26] L. Corradi *et al*., Z. Phys. A **335**, 55 (1990).
[27] S. Saha, Y. K. Agarwal, and C. V. K. Baba, Phys. Rev. C **49**, 2578 (1994).
[28] F. J. Schindler *et al*., Nucl. Phys. **A603**, 77 (1996).
[29] D. R. Napoli *et al*., Nucl. Phys. **A559**, 443 (1993).
[30] A. Shrivastava, S. Kailas, P. Singh, A. Chatterjee, A. Navin, A. M. Samant, V. Ramdev Raj, S. Mandal, S. K. Datta, and D. K. Awasthi, Nucl. Phys. **A635**, 411 (1998).